

COMPUTATIONAL CHALLENGES IN ESS

H. Danared, M. Eshraqi, E. Laface, R. Miyamoto, S. Molloy and A. Ponton,
European Spallation Source, Box 176, SE-221 00 Lund, Sweden

Abstract

The European Spallation Source, ESS, will be based on a 2.5-GeV, 50-mA superconducting proton linac delivering 5 MW of beam power to a rotating tungsten target. ESS is a challenging project in many respects, not the least with respect to RF power and RF sources. Because of the high power, relative beam losses must be very small to avoid activation and allow hands-on maintenance of accelerator components. The beam-dynamics calculations required to ensure these low beam losses are thus another challenge. This paper gives an introduction to ESS and the ESS linac, discusses briefly computational aspects in general, and presents specific examples of computational problems from beam dynamics and RF cavity design as well as efforts initiated to benchmark beam-dynamics codes for beam parameters relevant to ESS.

ESS AND THE ESS LINAC

Lund was selected as the site for the European Spallation Source, ESS, in 2009, and a year later, the ESS Accelerator Design Update, ADU, Project was launched. This project is a collaboration between universities and institutes in five European countries with additional participation and support from accelerator laboratories in many countries inside and outside of Europe. One of the primary outputs from the ADU Collaboration and of the ESS design effort as a whole will be a Technical Design Report at the end of 2012. This will be accompanied by a cost report, time schedule and other documents needed for the final approval of the construction of ESS.

Many of the parameters of the current ESS project [1] are similar to those of the ESS Design Study from 2003/2004 [2]. A major change is that the short-pulse source has been abandoned, based on studies showing that a large fraction of the science foreseen at ESS can be done as well or better with a long-pulse source [3]. Thus, no accumulator ring is required, and the linac can accelerate protons instead of H^- ions. Significant progress has also been made in the field of superconducting RF since 2003. As a consequence, the CCL copper cavities have been replaced by superconducting spoke cavities, and the output energy of the linac has increased while the

Table 1: Selected ESS Top-level Parameters

Parameter	Unit	Value
Average beam power	MW	5
Proton kinetic energy	GeV	2.5
Average macro-pulse current	mA	50
Macro-pulse length	ms	2.86
Pulse repetition rate	Hz	14
Maximum cavity surface field	MV/m	40

current has decreased.

Top-level parameters of the ESS linac are summarized in Table 1. The linac will accelerate 50 mA of protons to 2.5 GeV in pulses that are 2.86 ms long and come with a repetition rate of 14 Hz. This implies that the average beam power on the target will be 5 MW, as in the 2003 ESS study, and the peak power will be 125 MW. The linac will have a normal-conducting front-end up to 79 MeV followed by three families of superconducting cavities and a high-energy beam transport to the spallation target which will consist of a rotating tungsten wheel.

A go-ahead for construction is expected in early 2013. Then will follow an intense period of detailed design and prototyping. The most critical components are cry-modules and RF sources, where worldwide production capacity will be a limiting factor. Acceptance tests at the site in Lund and installation work in the linac tunnel and the klystron gallery will also be time-consuming. Nevertheless, the current plan calls for first neutrons from the spallation target in 2019.

LINAC DESIGN

The configuration of the current, May 2012 Baseline linac is shown schematically in Fig. 1, and selected linac parameters are listed in Table 2 [4]. The warm linac has contributions from INFN Catania, CEA Saclay, ESS-Bilbao and INFN Legnaro, the superconducting cavities and their cryomodules are designed at IPN Orsay and CEA Saclay, and the HEBT will come from ISA in Aarhus.

The 50-mA proton beam is produced in a pulsed microwave-discharge source on a platform at 75 kV. A low-energy beam transport, LEBT, with two solenoid

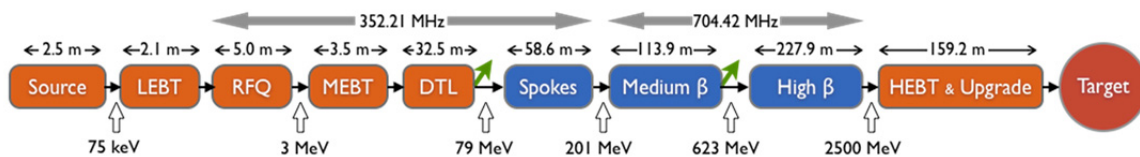


Figure 1: Schematic layout of the ESS linac [4]. Blue colour represents superconducting sections and green arrows locations where the beam could be extracted at intermediate energies.

Table 2: Selected Linac Parameters as of May 2012

Parameter	Device	Value
Length (m)	LEBT	2.1
	RFQ	5.0
	MEBT	3.5
	DTL	32.5
	Spokes	58.6
	Medium beta	113.9
	High beta	227.9
No. of cryomodules	Spokes	14
	Medium beta	15
	High beta	30
Cavities per module	Spokes	2
	Medium beta	4
	High beta	4
Optimal beta Geometrical beta	Spokes	0.50
	Medium beta	0.67
	High beta	0.92
Transition energy (MeV)	Source–RFQ	0.075
	RFQ–DTL	3
	DTL–spokes	79
	Spokes–medium beta	201
	Medium–high beta	623

magnets as focusing elements brings the beam to the entrance of the RFQ. The LEBT has a chopper that cuts away the beam while the proton pulses from the ion source stabilize, preventing a beam with off-nominal parameters from being accelerated in the RFQ and lost at high energy.

The 4-vane RFQ accelerates the beam to 3 MeV with small losses and a minimal emittance growth. It is designed specifically for ESS but it is based on the IPHI RFQ at Saclay. The RF frequency of the RFQ and the warm linac is 352.21 MHz.

After the RFQ there is a medium-energy beam transport, MEBT, with three buncher cavities and 10 quadrupole magnets. The MEBT has several different functions: it has optics to match and steer the beam from the RFQ into the drift-tube linac, it has a comprehensive set of beam-instrumentation devices, it has a chopper which acts faster than the LEBT chopper since space-charge neutralization is not an issue in the MEBT, and it allows collimation of the transverse particle distribution.

A drift-tube linac, DTL, with four tanks takes the beam from 3 MeV to 79 MeV. It has a FODO structure with permanent-magnet quadrupoles. Every second drift tube is empty or used for steering magnets and beam-position monitors.

The superconducting linac has three types of cavities: double-spoke resonators, five-cell medium-beta elliptical cavities and five-cell high-beta elliptical cavities. The May 2012 linac has 14 spoke cryomodules with two double-spoke resonators in each, and between the cryomodules there are warm quadrupole doublets. The spoke resonators operate at 352.21 MHz like the warm linac, but then there is a frequency doubling to the 704.42 MHz of the elliptical cavities. There are 15 medium-beta cryomodules with four cavities in each and

quadrupole doublets between, and there are 30 high-beta cryomodules with four cavities in each and quadrupole doublets between every second cryomodule.

All accelerating structures will be powered by klystrons, except the spoke resonators where tetrodes will be used. With one klystron per elliptical cavity plus a few for the warm linac, there will be close to 200 large klystrons and almost 100 modulators since one modulator will drive two klystrons. The density of components in the klystron building would become too high if these were to be positioned linearly. Instead they will be located in groups of eight klystrons and four modulators across the klystron building.

After the last cryomodule there is 100 m of tunnel where additional cryomodules can be installed for an energy upgrade. Then the beam is brought from the tunnel to the spallation target at the surface through two vertical bends and an expansion section. Quadrupole and octupole magnets are used to blow the beam up onto the desired profile of the proton-beam window and the target window.

SIMULATIONS AND BEAM DYNAMICS

Together with the large engineering efforts required to design, prototype, manufacture and install the accelerating structures and the massive RF system, one of the great challenges with the ESS linac is to accelerate and transport the 5 MW beam without losing more than about 1 W/m. This limit is set by activation, and a higher beam loss would make hands-on maintenance of the linac components difficult and time-consuming.

The design of the ESS linac uses beam-physics laws, rules-of-thumb and experience gained from past high-current linacs. Extrapolating from earlier machines, it seems reasonable to believe that the goal of losses of at most 1 W/m can be reached. Still, it is highly desirable to be able to use computational methods to predict beam loss and to verify that the lattice and the optics are optimal with respect to beam loss. This requires computational tools where all relevant physics is included, where non-linearities are taken into account to a sufficient degree, etc. The input from the linac design must be accurate, and in particular it must include misalignments, field errors and other static and dynamic deviations from the ideal linac. Simulations have to be performed from start to end, and the starting conditions must be well understood for the final result to be realistic. Losses of course occur from particles in the tails of the distributions, so these have to be modelled with high accuracy, generally requiring a large total amount of particles in the simulations, thus needing large amounts of cpu power. All in all, realistic simulations of beam losses are extremely demanding, and it is in fact not clear to us which level of accuracy one can reach.

The layout and optics of the ESS linac has so far been designed using the TraceWin suite of codes [5], although comparisons with other codes have been initiated (see below). Care has been taken to match the different sections of cavity families well to each other and to have

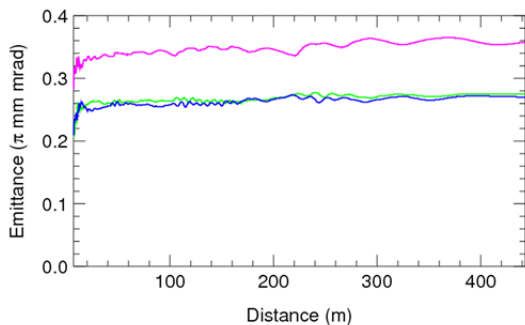


Figure 2: Normalized RMS emittances from the entrance of the MEBT to the end of the high-beta elliptical section in horizontal (green), vertical (blue) and longitudinal (violet) planes. The input distribution, at the entrance of the MEBT, is a 6D Gaussian truncated at 3 sigma with 0.21/0.21/0.28 π mm mrad.

a smooth phase advance in all planes. As an example of a result [6], the beam emittance in the three planes is plotted in Fig. 2, based on tracking of 100 000 macro particles. The RMS emittance is shown from the input of the MEBT until the end of the superconducting linac, and it is seen that the total emittance growth after the MEBT is not more than 10% in any of the planes. As already stated, however, predictions of beam loss need more aspects of the beam dynamics to be investigated, and, for instance, detailed error studies are going on at present.

Another example of beam-dynamics simulations for the ESS linac concerns the influence of unwanted cavity modes. Fundamental passband modes could prove to be dangerous due to their high R/Q compared to the accelerating modes at certain velocities. To explore this effect, a drift-kick-drift model was employed [7].

A pulse train of one million point-like bunches is tracked through the superconducting section of a linac, and the energy and time error generated by beam-induced modes is calculated. Figure 3 shows the resulting pulse phase space at the exit of two linacs with different velocity partitioning over the three cavity families [4, 8]. Of concern is when the growth due to passband modes (middle column) with respect to the case when no modes are acting (left column) is larger than that produced by

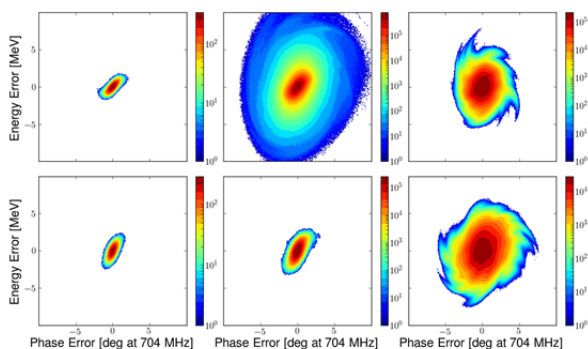


Figure 3: Pulse phase space at exit of two linacs (upper and lower rows) when no modes are acting (left), passband modes are acting (middle), there are uniformly distributed RF errors (right).

acceptable RF errors (right column). It can be seen that the linac of the top row, which represents an earlier ESS layout, is susceptible to these modes. The bottom row, corresponding to the present linac layout, shows significantly better performance.

CODE BENCHMARKING

Although TraceWin has been used so far for the ESS beam-dynamics calculations, an effort to compare the results with those of other codes has been initiated. Similar studies have been performed previously, see e.g. [9], but for different beam parameters. In the first phase, TraceWin, MADX-PTC [10, 11] and IMPACT [12] have been compared [13] with respect to acceleration and beam envelope in the transverse plane.

MADX-PTC

MADX is a widely used code for the design and study of accelerator rings as well as beam lines [10]. It does both calculation of lattice parameters and particle tracking. Complemented with the PTC library [11], MADX is capable of calculating six dimensional beam dynamics parameters and beam acceleration [14, 15]. Although the MADX and PTC already include the RF cavity as a lattice element, the included model does not have important details, such as the dependence of the longitudinal and transverse kicks on the transit time factor and its derivative as well as an offset between the electrical and mechanical centre. In our simulation with MADX-PTC, a finite length RF cavity is modelled as drift-kick-drift, where the kick includes a 4x4 thin-lens matrix modelling the transverse defocusing effect. Since a thin-lens matrix cannot be included in PTC, this simplified modelling limits us to use MADX only to study the transverse dynamics and PTC can be used to study only the longitudinal dynamics. To properly perform three-dimensional beam-dynamics calculations in a proton linac, it is ideal to develop a model of a finite length cavity with sufficient details together with the space charge effect, which is not included in the official version of MADX-PTC yet, under the framework of MADX-PTC in near future.

IMPACT

IMPACT is a particle tracking code developed at LBNL [12]. It uses a split-operator method based on a symplectic treatment of Hamilton's equations of motion and has options of both first and third order (Lorentz) integrators. In addition, it uses field maps for RF cavities, thus providing a more realistic form of tracking than codes based on the instantaneous kick-in-gap method. The space charge force is calculated using fast Fourier transform methods and a variety of boundary conditions are available. IMPACT has been regularly benchmarked with respect to other codes [9] and was also used to model the J-PARC and SNS linacs; as a result, the authors feel confident that it represents a suitable tool to check the results of the TraceWin. Comparison between the TraceWin and IMPACT is not straightforward due to

differences in conventions for the beam and lattice parameters and efforts are made to carry out a reliable comparison. The efforts include preparing a script to construct realistic field maps for drift tubes and cavities from the lattice file of the TraceWin and preparing another script to convert the relative cavity phase used by the TraceWin to the absolute cavity phase used by IMPACT based on iterative phase scanning.

Results

Figure 4 compares the kinetic energy of the beam at each longitudinal location starting from the entrance of the MEBT. The results from the TraceWin and PTC are from the lattice parameter calculations and that from the IMPACT is from tracking. The three codes are in very good agreement as it should be the case.

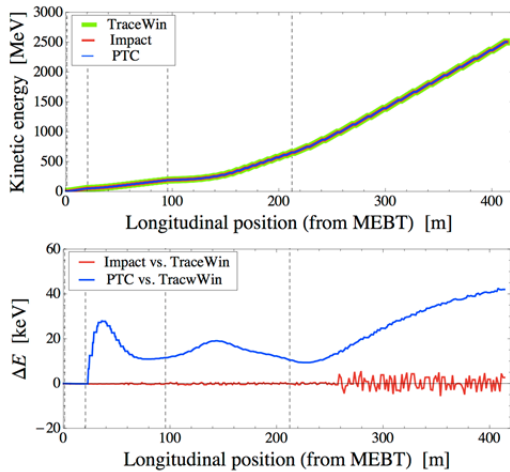


Figure 4: Comparison of kinetic energies calculated by TraceWin, IMPACT and MADX-PTC. Dotted lines represent transitions between two sections.

Figure 5 compares the transverse RMS beam size for the case of the zero current and hence with no effect of the space charge force. As the case of Fig. 2, the results from the TraceWin and MADX are from the lattice parameter calculations and that from the IMPACT is from the tracking. The third and fourth plots show the relative differences of the MADX and IMPACT with respect to the TraceWin. In TraceWin and MADX, each cell of a cavity is treated as drift-kick-drift but the kicks of the two codes are identical only up to the first order. This difference in the modelling generates the difference in the RMS sizes in the DTL. The amplitudes of $\Delta\sigma_x/\sigma_x$ and $\Delta\sigma_y/\sigma_y$ remain on the same level in sections following the DTL, suggesting the difference between TraceWin and MADX-PTC is only in the DTL and may not be significant. On the other hand, some discrepancies are evident between the TraceWin and IMPACT, considered to be due to the different orders of tracking and the use of field maps in the IMPACT but not in TraceWin.

A further comparison is in Fig. 6, which shows the transverse RMS beam sizes for the case of the full current (50 mA) based on the tracking with TraceWin and IMPACT. For the initial particle distribution, a six

ISBN 978-3-95450-116-8

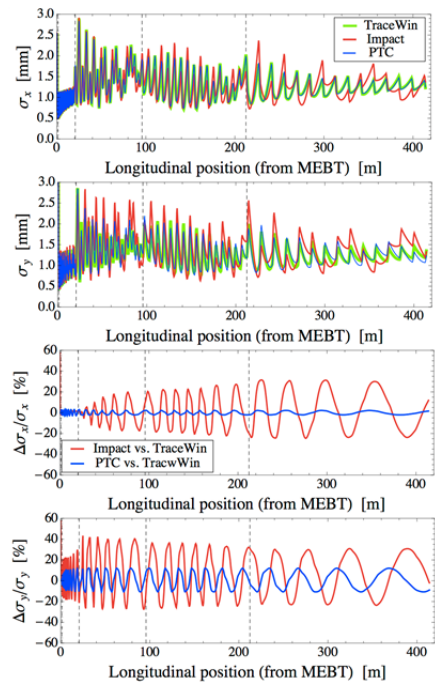


Figure 5: Comparison of RMS beam size calculated by TraceWin, IMPACT and MADX-PTC for zero current. Dotted lines represent transitions between two sections.

dimensional waterbag distribution is used. The nonuniformity of the oscillations, differences between the horizontal and vertical planes and general nonlinear growth are evident, suggesting that much needs to be done to optimize the system, not only for basic beam dynamics but also for non-linear effects.

These preliminary studies show that the three codes under consideration are in good agreement for the dynamics of the beam core in the linear regime. Nevertheless a campaign of more detailed code comparisons using the ESS linac must be performed in order to get confidence in understanding linear as well as the non-linear behaviour of the linac beam in cases both with and without errors.

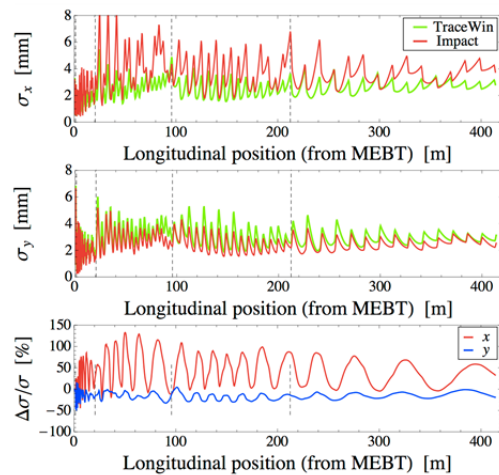


Figure 6: RMS beam envelope from IMPACT simulation with full space-charge.

COUPLER MULTIPACTOR

It is known that multipactor (MP) within higher order mode (HOM) couplers can cause considerable problems with the operation of high power superconducting cavities [16], and so it is of significant importance for the successful operation of ESS to understand any issues that may arise from installation of these couplers.

The development of a MP cascade within a coupler can have several effects, each of which may be catastrophic to the operation of the cavity:

- Absorption of the power within the accelerating mode of the cavity, thereby dropping its quality factor beyond acceptable limits.
- The increased thermal load due to absorption of the energy of the MP electrons can alter the physical geometry of the coupler, resulting in significant changes to its RF characteristics.
- A MP cascade between two points in the coupler introduces an additional conductive path in its equivalent circuit, and therefore totally changes its response to EM fields.

Note that the latter two effects result in the fundamental power being coupled out of these ports, resulting in the likely destruction of any attached electronics.

MP simulations using the ACE3P codes [17] have begun. The trajectories of electrons emitted around the inner walls of the couplers were simulated, with a postprocessing step involving scaling any resonances by a typical secondary electron yield for niobium (see Fig. 7).

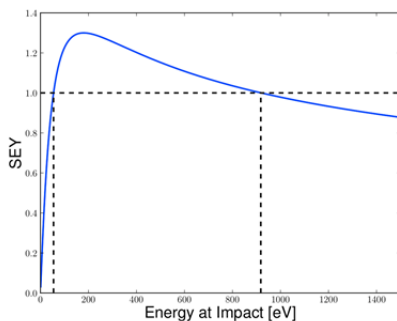


Figure 7: Secondary emission yield curve used in the postprocessing of simulation results.

Figure 8 shows a comparison of the MP behaviour of two HOM couplers proposed for use in ESS. It can be seen that one coupler displays very low-level, broad-band, MP, while the alternative has no broadband characteristics, however shows a very large, low energy, spike. Each of these effects could be catastrophic for the operation of the cavity, and so should be investigated in detail.

A remaining question relating to the computational aspects of this study is to what extent the assumptions relied on by the physics engine within this code impacts the final result. For example, the ACE3P codes always emit electrons normally to the cavity wall, and do not implement a statistical spread in the emission energy. In addition, they do not take account of space charge when

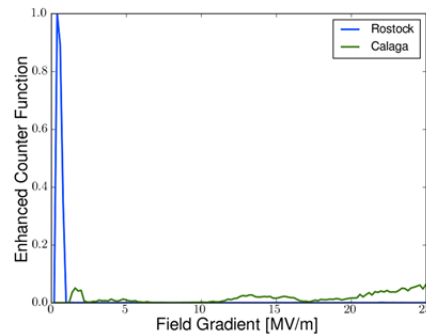


Figure 8: Comparison of the MP found in the two proposed HOM couplers [18].

tracking the emitted particles. Each of these effects may have a considerable effect on the outcome of the calculations.

MULTI-CAVITY FIELD EMISSION

As seen in [16], the statistics of the field emitted (FE) electrons impacting in the end-groups of a particular cavity are correlated with the settings of neighbouring cavities, implying that FE electrons are being transported throughout the cryomodule.

In order to investigate this effect, the ACE3P codes

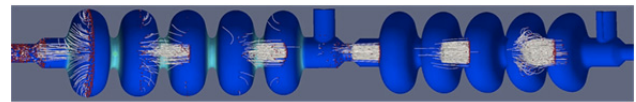


Figure 9: A simulation of FE trajectories in two cavities.

were used to track electrons emitted from the surface of one cavity throughout the volume enclosed by two cavities. This was done for a range of phase differences between the cavities in order to determine the effect on the impact locations of each of these electrons.

Figure 9 shows a frame from an animation of the transport of FE electrons by the accelerating field from the “most upstream” cell of one cavity into a

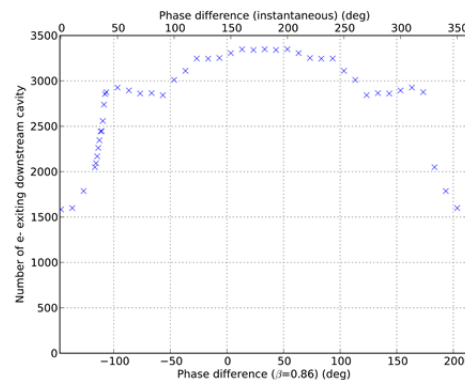


Figure 10: The integrated current emerging from the down-stream end of a two-cavity system plotted against their phase difference. The instantaneous phase difference (top axis), and that observed by a particle with $\beta = 0.86$ (bottom axis) is plotted.

neighbouring structure.

Figure 10 shows the dependence on phase difference of the current emerging from the downstream cavity. The ESS cavities will operate between approx. -80° and $+10^\circ$, and so should expect to see a high degree of FE activity spread throughout the cryomodules.

REFERENCES

- [1] ESS Conceptual Design Report, Ed. S. Peggs, ESS Report ESS-2012-1 (2012).
- [2] The ESS Project, Vol III, Technical Report, www.esss.se/documents/VolIII.pdf and ESS SC Reference Linac, Vol III Update Report, www.esss.se/documents/Chapt_1_Vol3upd.pdf.
- [3] F. Mezei, J. Neutron Res. **6** (1997) 3.
- [4] H. Danared, Proc. IPAC 2012, p. 2073.
- [5] R. Duperrier, N. Pichoff and D. Uriot, Proc. ICCS02, Springer-Verlag 2002, p. 411.
- [6] M. Eshraqi *et al.*, Proc. IPAC 2012, p. 3935.
- [7] M. Schuh *et al.*, Phys. Rev. ST Accel. Beams **14** (2011) 051001.
- [8] R. Ainsworth, Thesis in preparation, Royal Holloway, University of London.
- [9] L. Groening *et al.*, Proc ICAP 2009, p. 48.
- [10] F. Schmidt, G. Iselin and H. Grote, MAD-X, <http://mad.web.cern.ch>.
- [11] E. Forest, F. Schmidt and E. McIntosh, KEK-REPORT-2002-3.
- [12] J. Qiang *et al.*, J. Comp. Phys. **163** (2000) 434.
- [13] E. Laface *et al.*, Proc. IPAC 2012, p. 3841.
- [14] F. Schmidt *et al.*, CERN-AB-2005-036.
- [15] K. Skowronski *et al.*, Proc. ICAP 2006, p. 209.
- [16] S. Kim *et al.*, Proc. PAC 2007, p. 2511.
- [17] K. Ko *et al.*, Proc. LINAC 2010, p. 1028.
- [18] S. Molloy *et al.*, Proc. IPAC 2011, p. 190.